PERGAMON

International Journal of Heat and Mass Transfer 41 (1998) 3161–3176

International Journal of HEAT and MASS TRANSFER

A new turbulence model for near-wall natural convection

W. Xu[a,*], Q. Chen[a], F. T. M. Nieuwstadt[b]

[a] *Massachusetts Institute of Technology, 77 Massachusetts Avenue, Cambridge, MA 02139, U.S.A.*
[b] *Delft University of Technology, Rotterdamseweg 145, 2628 AL, Delft, The Netherlands*

Received 10 October 1997; in final form 17 February 1998

Abstract

Current turbulence models for simulating natural convection require too much computation time or do not give sufficiently accurate results. A one-equation near-wall model is developed that incorporates the use of direct numerical simulation data ($Ra = 5.4 \times 10^5$) to remedy these shortcomings. The use of this near-wall model along with the standard k-ε model for the outer-wall region, yields good predictions for mean flow and turbulence in natural convection and significantly reduces computational cost. © 1998 Elsevier Science Ltd. All rights reserved.

Nomenclature

A_μ, A_ε constants used in the one-equation models
$C_{1_\varepsilon}, C_{2_\varepsilon}, C_{3_\varepsilon}$ constants used in the ε equation
C_μ constant used for calculating ν_t
d_k diffusion of turbulent kinetic energy
g gravitational acceleration
g_i component i of the gravitation vector
G_k gravity production of turbulent kinetic energy, $-\beta g_i \overline{u_i t}$
Gr_x local Grashof number, $\beta g \Delta T x^3/\nu^2$
h convective heat transfer coefficient
k turbulent kinetic energy, $\overline{u_i u_i}/2$
L characteristic length
Nu_x local Nusselt number, hx/λ_{air}
P_k shear production of the turbulent kinetic energy, $-\overline{u_i u_j}\,\partial U_i/\partial x_j$
Pr Prandtl number
Pr_t turbulent Prandtl number
P_t total pressure
p fluctuating pressure
Ra Rayleigh number, $\beta g \Delta T L^2/\nu\lambda$
T mean temperature
T_a ambient temperature
t fluctuating temperature or time
U_i component i of the mean velocity
U, V, W mean velocity component in x, y and z direction
u, v fluctuating velocity component in x, y direction
u_i component i of fluctuating velocity
u_τ friction velocity, $\sqrt{\tau_\omega/\rho}$
$\overline{u_i u_j}$ Reynolds stress
$\overline{u_i t}$ turbulent heat flux
V_c characteristic velocity, $\sqrt{\beta g \Delta T L}$
x, y, z spatial coordinate
y_n normal distance to the nearest wall
y^+, y^*, y_v^* dimensionless wall distance, $y_n u_\tau/\nu$, $y_n\sqrt{k}/\nu$, y_n/ν.

Greek symbols
β thermal expansion coefficient, $-1/\rho\,\partial\rho/\partial T$
δ_{ij} Kronecker delta
ε turbulent energy dissipation
λ thermal conductivity
ν molecular viscosity
ν_t turbulent viscosity
π fluid density
σ_k, σ_ε Prandtl number of k and ε
τ_w wall shear stress.

Superscript
time-averaged quantities.

Subscripts
i, j spatial coordinate indices
ref reference conditions
t turbulent quantities.

* Corresponding author.

0017–9310/98 $19.00
PII: S0017-9310(98)00081-7

1. Introduction

1.1. Objectives of the current study

The prediction of buoyancy-affected flows, such as air movement in building enclosures, air flow around electronic equipment, and coolant flow in nuclear reactors, requires proper turbulence modeling. The turbulence models currently available, such as low-Reynolds-number k–ε models (LRN KEM) and Reynolds-stress models (RSM), demand either placing very fine grids in the near-wall region (in LRN KEM) or solving many differential equations simultaneously (in RSM). To and Humphrey [1] found that, for LRN KEMs, at least five grid points are needed in the viscous sublayer ($y^+ < 4$) and about 17 in the buffer region. Use of LRN KEM or RSM in three-dimensional applications requires a high-speed computer that is not available for most engineers. Hence, it is necessary to develop an accurate, cost-effective turbulence model for calculating buoyancy-affected flows.

In this paper, we propose a new two-layer turbulence model for simulating buoyancy-induced air flows. The development of this model has employed the direct numerical simulation (DNS) data from a recent study [2]. The DNS data are used to conduct a term-by-term assessment of the turbulent kinetic energy equation and to develop a new one-equation *near-wall* model. This near-wall model, together with the standard KEM [3] or RSM for the region away from walls, can reduce computing cost considerably. The near-wall region requires only 7–10 grid points to produce acceptable results, compared with 20–30 points needed by a LRN KEM. This new model has been used to calculate four natural convection flows, and the results have been compared with DNS or experimental data.

1.2. Earlier work

1.2.1. Experimental studies

Many experimental studies of turbulent natural convection have been performed during the last two decades. These experiments fall into two major categories: turbulent boundary layer flows and turbulent cavity flows. Pioneering experimental studies of the turbulent boundary layer flows were by Warner and Arpaci [4] and Cheesewright [5]. These authors primarily measured the overall heat transfer and mean flow quantities. Measurements of turbulent structures were provided by Smith [6] and Cheesewright and Doan [7], who used hot-wire anemometers, and Miyamoto and Okayama [8], who used laser Doppler velocimeters (LDV). Tsuji and Nagano [9, 10], systematically investigated mean flow characteristics and turbulence quantities, such as Reynolds-stresses, by using the V-shaped hot-wire technique. Their measurements are highly reliable and have been used by many other researchers [11, 12].

Turbulent natural convection in cavities was first investigated experimentally by Elder [13], Giel et al. [14], and Cowan et al. [15]. However, the experiments were conducted using water rather than air and did not include measurements of turbulent quantities. Cheesewright et al. [16] measured the mid-height's mean velocities, the core temperature profile and some turbulence statistics in an air-filled room with differentially heated walls. The Rayleigh number studied is on the order of 10^{10}. Olson et al. [17] performed an experiment of natural convection in an air-filled room and in a small-scale model with and without partitions, with a Rayleigh number on the order of 10^{10}. They visualized the flow and measured the temperatures in the core and wall boundary layer. Secondary recirculating loops were found in their experiments. Recently, Dafa'Alla and Betts [18] conducted measurements in a tall, air-filled cavity with an aspect ratio 28.6 and a Rayleigh number of 8.3×10^5 based on the cavity width. They used a laser Doppler anemometer to measure the velocity and velocity fluctuations, thermocouples to measure the temperature and temperature fluctuations.

These experimental investigations are essential to validate numerical models. Once validated experimentally, the numerical models are less expensive and can provide more detailed information about the buoyant flows than the available experimental method.

1.2.2. Numerical simulations

Similar to the experimental studies, the numerical investigations may also be classified according to *turbulent boundary layer* and *turbulent cavity* flows. Contributions to the numerical studies of turbulent natural convection along a vertical, heated, flat plate are due to To and Humphrey [1], Henkes and Hoogendoorn [19], Peeters and Henkes [20], and Yuan et al. [11], among many others. To and Humphrey employed a LRN KEM; Henkes and Hoogendoorn adopted an algebraic model and several LRN KEMs; Peeters and Henkes used a RSM; and Yuan et al. used a KEM with wall functions derived from the experimental data in ref. [9, 10]. Results from these works indicate that the LRN KEM, RSM and standard KEM with proper wall-boundary modeling are able to predict mean flow. However, the computations require either the use of very fine grids or the solution of many differential equations.

Contributions to the numerical simulation of natural convection flows in cavities include those of Henkes et al. [21], Chen [22], Lankhost et al. [23], and Hanjalic et al. [24]. Henkes et al. [21] used the standard KEM and several LRN KEMs to simulate natural convection in a differentially heated, air-filled, square cavity with Rayleigh numbers up to 10^{14}. They found that the standard KEM overpredicts wall heat transfer but that the LRN KEMs provide more accurate predictions. Chen [22] employed several RSMs to calculate the natural, forced and mixed convection flows in rooms and found the

performance of the different RSMs was similar. His results agreed with mean flow measurements but showed less satisfactory agreement for the turbulent quantities. Lankhost et al. [23] made use of the standard KEM and wall functions to simulate air flows in a room with a radiator. They used wall functions to determine k and ε but abandoned the wall functions when determining velocity and temperature. A very find grid distribution was necessary to resolve the large gradients of velocity and temperature in the boundary layers. The Rayleigh number in their study was about 3×10^{10}. Hanjalic et al. [24] applied a three-equation and a four-equation model, $k-\varepsilon-\overline{\theta^2}$ and $k-\varepsilon-\theta^2-\varepsilon_\theta$, and incorporated LRN modifications to calculate air flows in several empty and partitioned rooms. The Rayleigh numbers in their study ranged from 10^{10}–10^{12}, which is the range observed in building enclosures. Their computed mean temperatures and velocities agreed with the corresponding experimental data.

For most of the above numerical simulations to provide satisfactory results, they must use fine grids in boundary layers or solve many transport equations.

1.2.3. Direct numerical simulations

DNS has drawn much interest in recent years. Phillips [25], used DNS to calculate the turbulent natural convection in a differentially heated vertical slot at a Rayleigh number 1.57×10^5. Paolucci [26], investigated the natural convection in a square cavity by DNS with Rayleigh numbers up to 10^{10}. Xin et al. [27] computed flows in two cavities with aspect ratios of 1 and 4 and Rayleigh numbers up to 10^{10}. A recent study conducted by Versteegh and Nieuwstadt [2] computed the natural convection along a pair of infinite plates at a Rayleigh number of 5.4×10^5. An independent study by Boudejemadi et al. [28] confirmed the results from Versteegh and Nieuwstadt. Dol et al. [29] pointed out that the study by Boudejemadi et al. used a shorter spanwise length in the simulation, which has artificially enhanced the turbulence level. Both DNS results [2, 28] are also confirmed by a recent experiment in a tall cavity with aspect ratio of 28.6:1 [18].

Due to the simplicity of the geometry and reliability of the data in the study by Versteegh et al. [2], we have chosen to employ their results to perform a term-by-term assessment of the k-equation model and develop a new one-equation near-wall model for computing turbulent natural convection.

2. One-equation modeling in the near-wall region

The flow geometry on which the DNS [2] was performed is shown in Figs 1 and 2, in particular, show the results of $Ra = 5.4\times10^5$.

The DNS data indicate that some near-wall characteristics of natural convection are quite different from those of forced convection. Figure 1b shows that the local equilibrium (shear production over dissipation) is not established. Figure 1c indicates that the well-known log-law velocity profile is not valid in the boundary layer of the natural convection. These significant differences suggest the need for a detailed analysis of the near-wall one-equation model.

2.1. Assessment of the k-equation models

Eddy-viscosity concept requires a length scale and a velocity scale in order to compute the eddy-viscosity. In one-equation turbulence models, the length scales are usually obtained empirically and the velocity scale is obtained by solving the turbulent kinetic energy equation: k-equation. The exact (without turbulence modeling) k transport equations reads

$$\frac{\partial k}{\partial t}+U_i\frac{\partial k}{\partial x_i}=d_k+P_k+G_k-\varepsilon \tag{1}$$

where

$$d_k=\frac{\partial}{\partial x_k}\left(-\frac{\overline{u_iu_iu_k}}{2}+\frac{1}{\rho}\overline{pu_k}+\nu\frac{\partial k}{\partial x_k}\right) \tag{2}$$

represents total diffusion contribution from turbulence, pressure and viscous transport. The shear production term reads

$$P_k=-\overline{u_iu_j}\frac{\partial U_i}{\partial x_j}. \tag{3}$$

The buoyancy production/destruction term is

$$G_k=\frac{1}{\rho}\frac{\partial\rho}{\partial T}g_i\overline{u_it} \tag{4}$$

If the overheat ratio $\Delta T/T_{ref}$ is small, the Boussinesq assumption is valid and the buoyancy term can be further simplified to

$$G_k=-\beta g_i\overline{u_it} \tag{5}$$

where g_i is the gravity vector component and β is the thermal expansion coefficient. The last term of equation (1), denoted as ε, represents turbulence dissipation:

$$\varepsilon=\nu\overline{\frac{\partial u_i}{\partial x_j}\frac{\partial u_i}{\partial x_j}} \tag{6}$$

The DNS data gives the budgets of the k-equation as shown in Fig. 1d. In the region where $y^+<2$, the viscous diffusion and the dissipation are dominant and balance each other. The region $2<y^+<10$ has a negative shear production. Gravity production is positive in this region. For large value of y^+ (>40), shear production becomes positive and actually dominated over gravity production.

The exact k-equation introduces the following unknown quantities: $\overline{u_iu_iu_k}$, $\overline{pu_i}$, $\overline{u_iu_j}$, $\overline{u_it}$ and ε. Unless additional transport equations are introduced to solve for these quantities, these quantities have to be modeled.

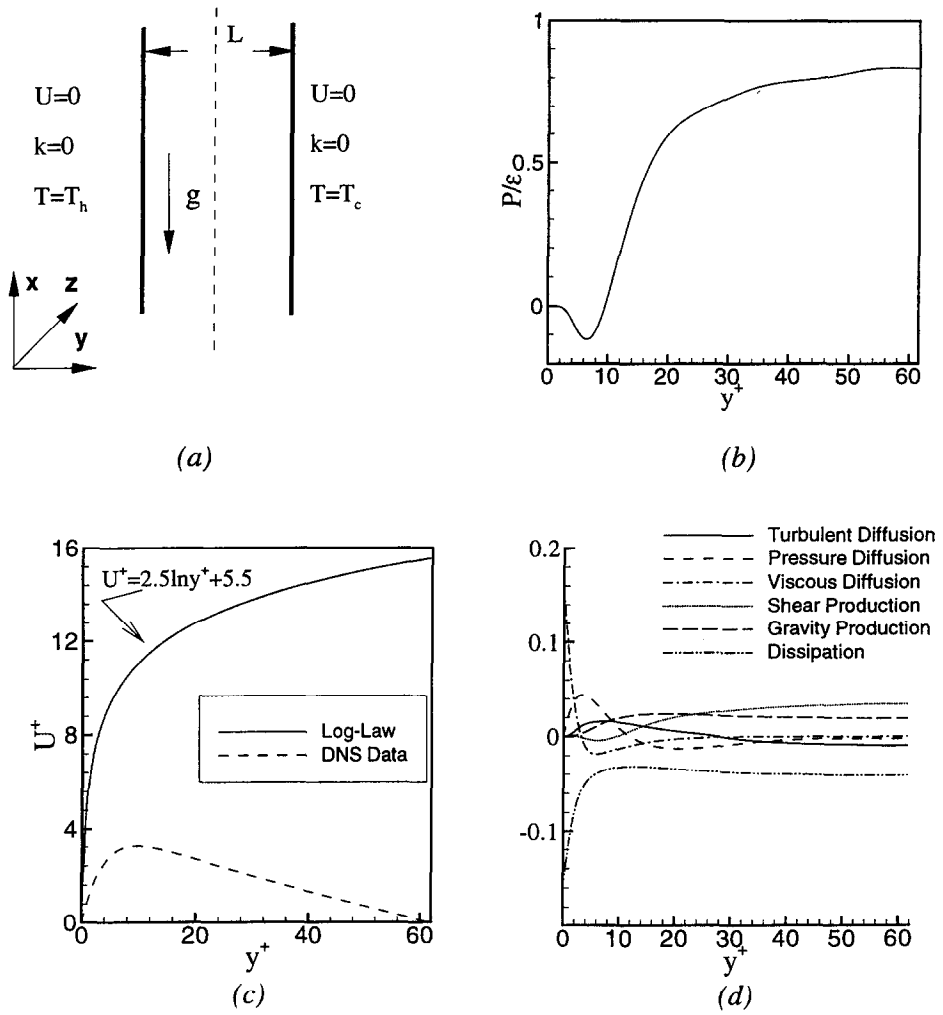

Fig. 1. Analysis of the boundary layer of natural convection. (a) The geometry and boundary conditions of a pair of infinitely long plates; (b) the ratio of shear production and dissipation; (c) velocity profiles; (d) k-equation budgets.

The left-hand-side of the exact k-equation is known, and it does not require modeling. The right-hand-side terms and their models are listed in Table 1. The modeled forms are obtained by substituting the following eddy-viscosity assumptions into the exact form:

$$-\frac{1}{2}\overline{u_i u_i u_j}+\frac{1}{\rho}\overline{pu_j}=\frac{v_t}{\sigma_k}\frac{\partial k}{\partial x_j} \tag{7}$$

$$-\overline{u_i u_j}=v_t\left(\frac{\partial U_i}{\partial x_j}+\frac{\partial U_i}{\partial x_j}\right)-\frac{2}{3}\delta_{ij}k \tag{8}$$

$$-\overline{u_i t}=\frac{v_t}{Pr_t}\frac{\partial T}{\partial x_i} \tag{9}$$

$$\varepsilon=\frac{k^{3/2}}{l_\varepsilon} \tag{10}$$

The eddy viscosity is computed by

$$v_t=C_\mu\sqrt{k}l_\mu \tag{11}$$

Applying the following conditions:

$$\frac{\partial}{\partial x}=0,\quad \frac{\partial}{\partial z}=0V=W=0 \tag{12}$$

which are appropriate for the configuration shown in Fig. 1a, to the modeled forms, yields the expanded form shown in Table 1.

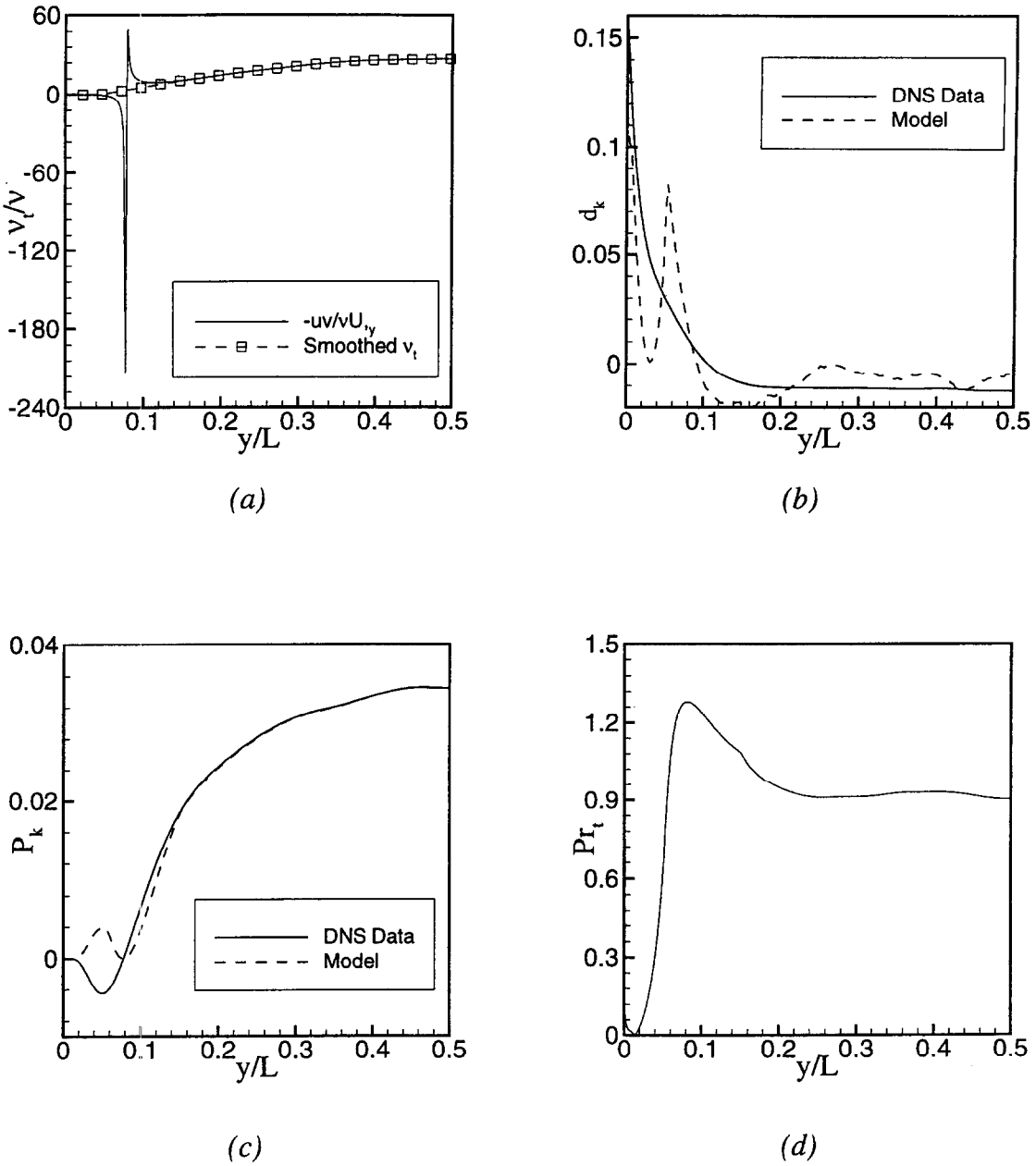

Fig. 2. Analysis of the k-equation. (a) ν_t; (b) d_k; (c) P_k; (d) Pr_t (DNS data).

In order to examine the accuracy of these models, we have conducted a term-by-term evaluation of the k-equation models. This evaluation uses the DNS data to determine the exact and modeled forms. Equations (7)–(9) introduce the eddy-viscosity term. If the ν_t calculated from the DNS data by:

$$\nu_t = -\overline{uv}\Big/\frac{dU}{dy} \tag{13}$$

there are negative values and two sharp peaks in the ν_t distribution (see Fig. 2a), which would not occur by using equation (11). This is due to so-call counter-diffusion phenomenon and the velocity maximum. A positive and smoothed ν_t, as shown in Fig. 2a, has been used for this investigation. Figure 2b compares the diffusion term with its model. In most of the region, the eddy-viscosity model could describe the diffusion term, although the modeled d_k is not as smooth as the exact one. Figure 2c gives the

Table 1
The exact, modeled and expanded form of the k-equation

	Exact form	Modeled form	Expanded form
Turbulence diffusion	$\frac{\partial}{\partial x_j}\left(-\frac{\overline{u_i u_i u_j}}{2}\right)$		
Pressure diffusion	$+\frac{1}{\rho}\frac{\partial \overline{pu_j}}{\partial x_j}$	$\frac{\partial}{\partial x_j}\left[\left(\nu+\frac{\nu_t}{\sigma_k}\right)\frac{\partial k}{\partial x_j}\right]$	$\frac{\partial}{\partial y}\left[\left(\nu+\frac{\nu_t}{\sigma_k}\right)\frac{\partial k}{\partial y}\right]$
Viscous diffusion	$+\frac{\partial}{\partial x_j}\left(\nu\frac{\partial k}{\partial x_j}\right)$		
Shear production	$-\overline{u_i u_j}\frac{\partial U_i}{\partial x_j}$	$\nu_t\left(\frac{\partial U_i}{\partial x_j}+\frac{\partial U_j}{\partial x_i}\right)\frac{\partial U_i}{\partial x_j}$	$\nu_t\left(\frac{\partial U}{\partial y}\right)^2$
Gravity production	$-\beta g_i \overline{u_i t}$	$\beta g_i \frac{\nu_t}{Pr_t}\frac{\partial T}{\partial x_i}$	0
Dissipation	$\nu\overline{\frac{\partial u_i}{\partial x_j}\frac{\partial u_i}{\partial x_j}}$	$\frac{k^{3/2}}{l_\varepsilon}$	$\frac{k^{3/2}}{l_\varepsilon}$

comparison of the shear production calculated by the exact and modeled form. The modeled form agrees with the DNS data fairly well, except that the negative production cannot be reproduced, since the shear production term in the expanded form,

$$\nu_t\left(\frac{\partial U}{\partial y}\right)^2,$$

cannot be negative.

The gravity production term, $-\beta g_i \overline{u_i t}$, as shown in Table 1, disappears after applying equation (9) to the unstratified temperature distribution. This problem has also been noted in several previous studies on the vertical boundary layers of the natural convection [1, 20], where

$$\frac{\partial}{\partial x} \ll \frac{\partial}{\partial y}.$$

Mason et al. [31] proposed

$$-\beta g_i \overline{u_i t} = \beta g_i \frac{\nu_t}{Pr_t}\frac{\partial T}{\partial y}$$

and Plumb et al. [32] suggested $-\beta g_i \overline{u_i t} = \beta g_i \sqrt{\overline{t^2} k}$.

Their proposals are suitable for some particular cases but are not universal. Hanjalic and Vasic [33] introduced an algebraic equation to solve for $\overline{u_i t}$ and obtain satisfactory results for the natural convection in cavities but with extra computational efforts. To and Humphrey [1] concluded that using gravity production term as zero has a small influence on the mean quantities, but leads to 7% underprediction of k. The present investigation uses equation (9) as the buoyancy production model.

Equation (9) can also be used to determine the turbulent Prandtl number. Figure 2d shows Pr_t computed by

$$Pr_t = \nu_t \frac{\mathrm{d}T}{\mathrm{d}y}\Big/ -\overline{vt}$$

from the DNS data. As y^+ decreases in the range $0 < y^+ < 15$, the Pr_t decreases as well. This differs from the well-known behavior of Pr_t in forced convection where Pr_t *increases* beyond 1 as y^+ decreases in the $0 < y^+ < 10$ [30]. However, Pr_t approaches 0.9 when y^+ exceeds 30. Henkes et al. [19] found that increasing Pr_t from 0.9 to 1.0 leads to just 5% difference in the wall heat transfer. They concluded that Pr_t had only a small effect on the results. These facts suggest that a constant value of 0.9, which is also used by To and Humphrey [1], is still a reasonable choice. Therefore, it is also used in the present investigation.

The last term on the right-hand-side of equation (1), ε, represents the turbulent energy dissipation and will be discussed in the next section since it involves the modeling of length scales.

2.2. Assessment of the length scales models

To compute the dissipation and eddy viscosity, two length scales need to be specified. For the near-wall region, the length scales used in the one-equation models often follow the Van Driest's damping law as:

$$l_\mu = C_l y_n (1 - \exp(-y^*/A_\mu)) \tag{14}$$

$$l_\varepsilon = C_l y_n (1 - \exp(-y^*/A_\varepsilon)) \tag{15}$$

where C_l, A_μ and A_ε are model constants. The use of $y^* = \sqrt{k} y_n/\nu$ here, rather than y^+, can extend the application of equations (14) and (15) to separated flows [35]. Norris and Reynolds [34] proposed a different form for l_ε:

$$l_\varepsilon = \frac{C_l y_n}{1+5.3/y^*} \tag{16}$$

Durbin [36] and Rodi et al. [37], suggested using the square root of the wall-normal stress $\sqrt{\overline{vv}}$ instead of $\sqrt{k}$ as a velocity scale. Based on this suggestion, Rodi et al. proposed:

$$l_\mu = 0.33 y_n \tag{17}$$

$$l_\varepsilon = \frac{1.3 y_n}{1+2.12/y_v^*} \tag{18}$$

where

$$y_v^* = \frac{y_n\sqrt{\overline{vv}}}{\nu}.$$

Note that the formulas used to compute ν_t and ε are changed to

$$\nu_t = \sqrt{\overline{vv}}\, l_\mu \tag{19}$$

$$\varepsilon = \frac{\sqrt{\overline{vv}}\, k}{l_\varepsilon} \tag{20}$$

where $\overline{vv}$ is calculated by an algebraic equation given in Ref. [37].

Rodi [35] found encouraging results with the two-layer models (applying the above equations (14) or (17) for l_μ, and (15) or (16) or (18) for l_ε, with (19) and (20) for ν_t and ε, to the near-wall region and the standard KEM or a RSM to the outer region). The two-layer models use less grid points than LRN KEMs and are more accurate than the wall functions. However, most of the one-equation models were developed for forced convection flows such as isothermal channel or boundary layer flows. In forced convection, the structure parameter $\overline{uv}/k$ is commonly believed to be approximately 0.3 under local equilibrium conditions. However, Fig. 3a shows that $\overline{uv}/k$ in natural convection is not a constant. Furthermore, using the DNS data, Fig. 3b compares l_μ of Van Driest's damping law (equation (14)) with the l_μ from equation (11) with DNS data. Figure 3c compares the l_μ proposed by Rodi et al. [37] (equation (17)) for forced convection flows, with the exact l_μ determined from equation (19). Clearly, the Van Driest's damping law and Rodi's model could not predict the l_μ in natural convection. Figure 3d further compares the l_ε calculated from Van Driest's damping law (equation (15)) and the Norris and Reynolds' model (equation (16)) with the exact l_ε determined from equation (10). The l_ε proposed by Rodi et al. (equation (18)) is compared with the exact l_ε determined from equation (20). The comparisons show that equations (15), (16) and (18) are not appropriate for the natural convection boundary layers. Thus, it is necessary to derive a new near-wall model for natural convection.

2.3. A new one-equation near-wall model

2.3.1.

Modeling l_μ and l_ε. For the near-wall region, Durbin [36] suggested using $\sqrt{\overline{vv}}$ as the velocity scale in order to avoid artificial damping functions in the length scales. Rodi et al. [37] applied this concept to develop equations (17) and (19) for the channel and boundary layer flows of forced convection. For natural convection flows, the DNS data gives the profiles of l_μ and l_ε shown in Fig. 3c and e. The following equations can fit these profiles fairly well:

$$l_\mu = \frac{0.544 y_n}{1+5.025\times10^{-4} y_v^{*1.65}} \tag{21}$$

$$l_\varepsilon = \frac{8.8 y_n}{1+10/y_v^*+5.15\times10^{-2} y_v^*} \tag{22}$$

where

$$y_v^* = \frac{y_n\sqrt{\overline{vv}}}{\nu}.$$

The new l_μ and l_ε are shown in Fig. 3c and e, respectively. Note that equation (22) correctly retains the characteristics of ε near the wall: $\varepsilon \propto y^0$ [37].

2.3.2. *Modeling of* $\overline{vv}$

Introducing $\overline{vv}$ to the one-equation model requires an additional correlation between $\overline{vv}$ and k. The DNS data give the $\sqrt{\overline{vv}}$ profile shown in Fig. 3f. The following curve-fitting formula is used in the present study:

$$\frac{\overline{vv}}{k} = 7.19\times10^{-3} y^* - 4.33\times10^{-5} y^{*2} + 8.8\times10^{-8} y^{*3} \tag{23}$$

Since the available DNS data are obtained under particular geometry and Rayleigh number, equations (21)–(23) need further validation for other geometry and conditions. The form of these formula might not be unique. However, as long as the correlation holds in most natural convection boundary layer, equations (21)–(23) can still be safely used.

2.4. A new two-layer model

The proposed one-equation model solves only one transport equation (the modeled form of the equation shown in Table 1) and calculates $\overline{vv}$ with equation (23), l_μ with equation (21), l_ε with equation (22), and obtains ν_t, and ε with equations (19) and (20). This new model is applicable in the near-wall region. In the outer region, one could employ the standard KEM, i.e., k is solved by

$$\frac{Dk}{Dt} = \frac{\partial}{\partial x_i}\left(\left(\nu+\frac{\nu_t}{\sigma_k}\right)\frac{\partial k}{\partial x_i}\right) + \nu_t\left(\frac{\partial U}{\partial x_j}+\frac{\partial U_j}{\partial x_i}\right) - \varepsilon + g_i\beta\frac{\nu_t}{Pr_t}\frac{\partial T}{\partial x_i} \tag{24}$$

where $\sigma_k = 1.0$. The ε is not calculated by equation (20) but solved by a transport equation:

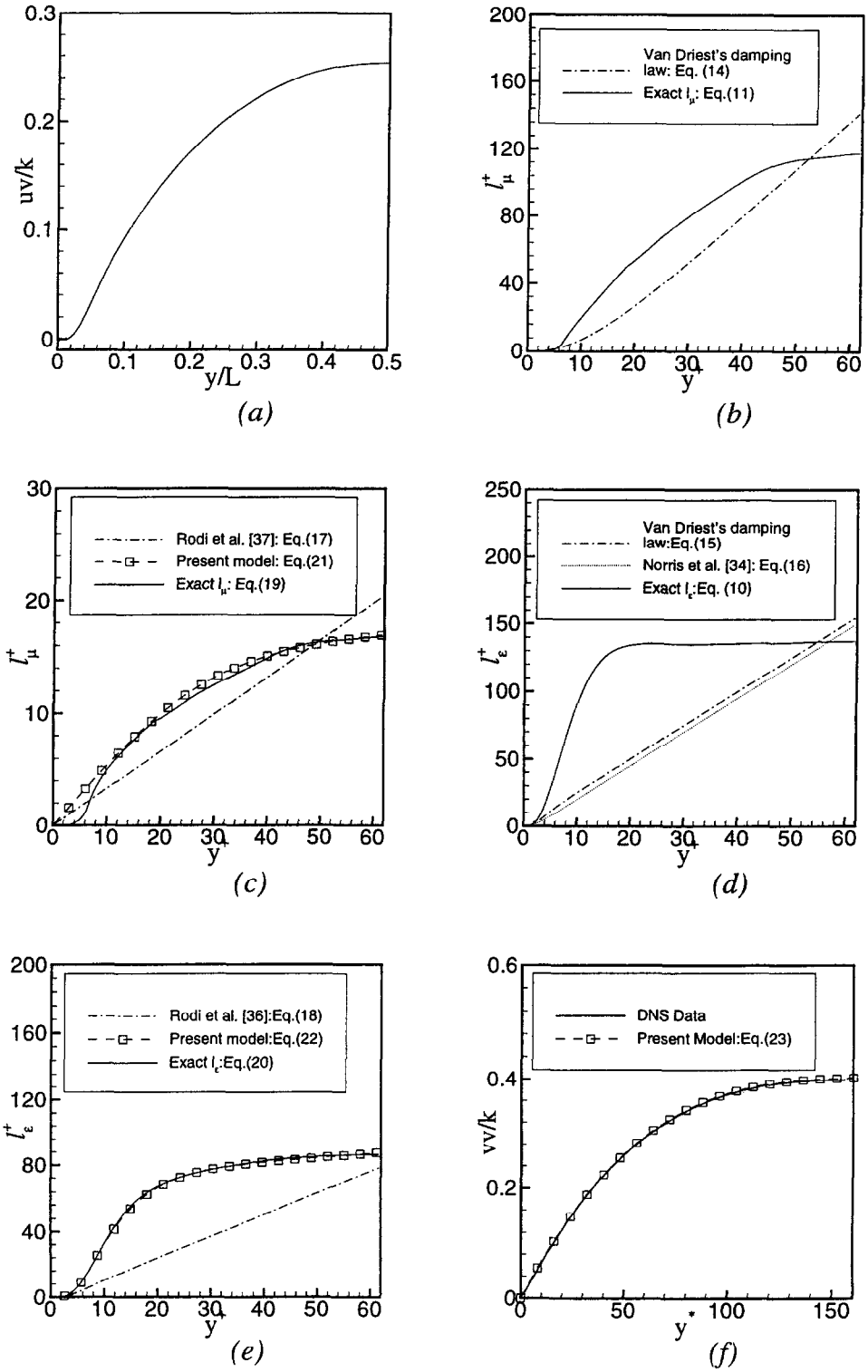

Fig. 3. Comparison of the one-equation near-wall models. (a) $\overline{uv}/k$; (b) dimensionless length scale $l_\mu^+ = l_\mu u_\tau/\nu$; (c) dimensionless length scale l_μ^+; (d) dimensionless length scale $l_\varepsilon^+ = l_\varepsilon u_\tau/\nu$; (e) dimensionless length scale l_ε^+; (f) $\overline{vv}/k$.

$$\frac{D\varepsilon}{Dt}=\frac{\partial}{\partial x_i}\left(\left(\nu+\frac{\nu_t}{\sigma_\varepsilon}\right)\frac{\partial\varepsilon}{\partial x_i}\right)+\frac{\varepsilon}{k}\left[C_{1\varepsilon}\nu_t\left(\frac{\partial U_i}{\partial x_j}+\frac{\partial U_j}{\partial x_i}\right)-C_{2\varepsilon}\varepsilon+C_{3\varepsilon}g_i\beta\frac{\nu_t}{Pr_t}\frac{\partial T}{\partial x_i}\right] \quad (25)$$

where $\sigma_\varepsilon = 1.3$, $C_{1\varepsilon} = 1.44$, $C_{2\varepsilon} = 1.92$, $C_{3\varepsilon} = 1.44$. Again, the ν_t in equations (24) and (25) is not calculated by equation (19) but by $\nu_t = C_\mu k^2/\varepsilon$, where $C_\mu = 0.09$. A new two-layer model can be easily formed by using the one-equation model in the near-wall region and the standard KEM in the outer region. Other combinations, such as using a RSM in the outer-wall region or using an algebraic flux model (e.g. the one developed by Hanjalic and Vasic [33]) for calculating buoyancy production, are also possible and will extend the application of the two-layer model to more complex buoyancy-driven flows.

In the present study, the two-layer model consists of the one-equation model within $y^* \leqslant 160$ and the standard KEM for $y^* > 160$. The reason to use $y^* = 160$ as a switching criterion is that the new one-equation model is consistent with the DNS data [2] within $y^* \leqslant 160$ (or $y^+ \leqslant 60$), as shown in Fig. 3. Hereafter, this switching method is defined as a y^*-prescription method. The y^*-prescription method is also used in the two-layer models for forced convection (Rodi et al. [37]). The forced convection has a higher y^* in the outer region than in the near-wall region and thus ensures that the models will be switched as desired. However, for natural convection, portion of the switching may not occur due to small y^* in the laminar outer region. To solve this problem, two alternatives could be considered:

(1) to use y^+ (≈ 60) instead of y^* as the model-switch criterion;
(2) to match two models at pre-selected grid lines running along the wall.

Method 1 does not apply to separated flow since $y^+ = 0$ at the separation point. Method 2 requires preknowledge of the flow, since the selection of the switch lines leans heavily on experience. Furthermore, we found that the results of the method 2 and the y^*-prescription method does not differ significantly. In the applications of the LRN KEMs in natural convection flows, such as in Refs [1, 19], the damping functions designed for resolving the wall-damping effects were also used in the outer region. Therefore, the $y^* = 160$ rule is used in the present study.

The following section will describe the application of the new two-layer model with the y^* prescription method to several natural convection cases.

3. Applications of the new two-layer model

Four natural convection cases were selected to validate the new two-layer model:

(1) natural convection along two vertical, parallel, infinitely long plates (Fig. 1a).
(2) natural convection along a heated, vertical, flat plate (Fig. 5a).
(3) natural convection in a cavity with an aspect ratio of 5 (Fig. 6a).
(4) natural convection in a room with differentially heated vertical walls and an aspect ratio of 2.5 : 7.9 (Fig. 7a).

A commercial CFD code, PHOENICS [38], was extended to include the two-layer model described in the previous section and was used for the validation. By default, PHOENCIS uses the finite-volume method. The differential method for the convection term of all differential equations used the upwind-difference-scheme. Staggered grids and SIMPLEST [38] method were used for decoupling the pressure and velocity fields. Grid distribution adopts the power-law spacing method [38]. The grid numbers and the values of the power are listed in Table 2. The under-relaxation used liner relaxation for the pressure and false-time-step method [38] for all other variables. The value of the under-relaxation factors are also provided in Table 2. The convergence criterion was set such that the respective sums of the absolute residuals of sources of U, V, P, T, k and ε must be less than 10^{-3}, where P actually refers to the continuity equation.

3.1. Natural convection along two vertical, parallel, infinitely long plates

The geometry and boundary conditions of this case are shown in Fig. 1a. This configuration corresponds to a very tall differentially heated cavity with negligible influence from the horizontal walls. As a very rare case in practice, little experimental data were available until the recent contributions from Dafa'Alla and Betts [18]. The Rayleigh number is 5.4×10^5 based on the distance between two plates. The DNS performed by Versteegh and Nieuwstadt [2] uses the same geometry and Rayleigh number.

Equation (12) is applicable since the plates are infinitely long in both the x and z directions. Hence the case can be simplified to a 1-D problem so that only the boundary conditions at the plates need to be specified. At the plates, the no-slip and fixed temperature boundary conditions holds for the velocity U the temperature T, respectively. The turbulent kinetic energy is zero at the plates. The turbulence dissipation rate ε is determined from equation (20). Since $\overline{vv} \propto y^4$ and $k \propto y^2$, the use of equations (20) and (22) implies $\varepsilon \propto y^0$ as y goes to zero. It is worth mentioning that an estimation of ε value at wall

$$\varepsilon = 2\nu\left(\frac{\partial k^{1/2}}{\partial y}\right)_w^2$$

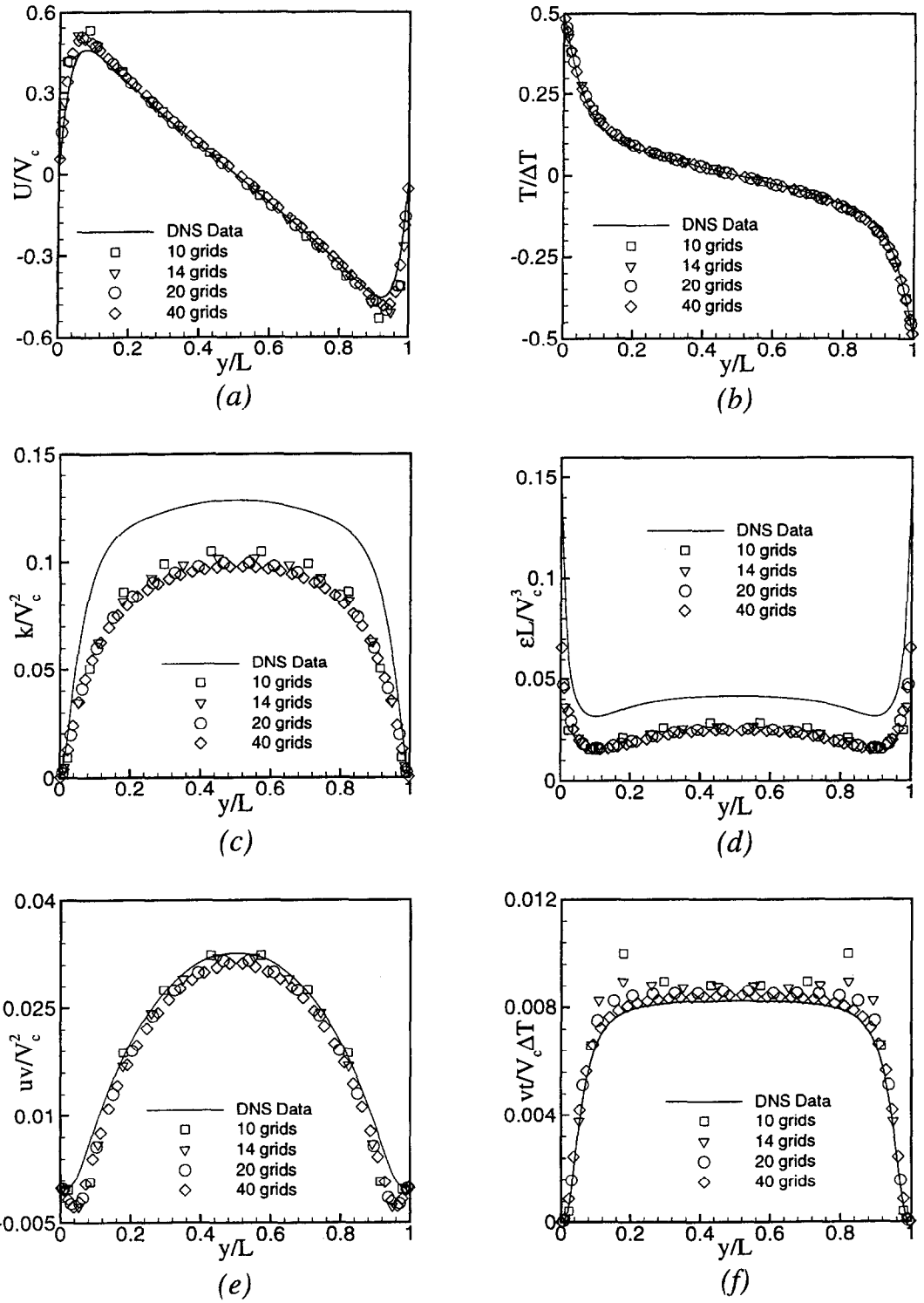

Fig. 4. Natural convection between two infinitely long plates. (a) Mean velocity; (b) mean temperature; (c) turbulent kinetic energy; (d) turbulent dissipation; (e) shear-stress $\overline{uv}$; (f) turbulent heat flux.

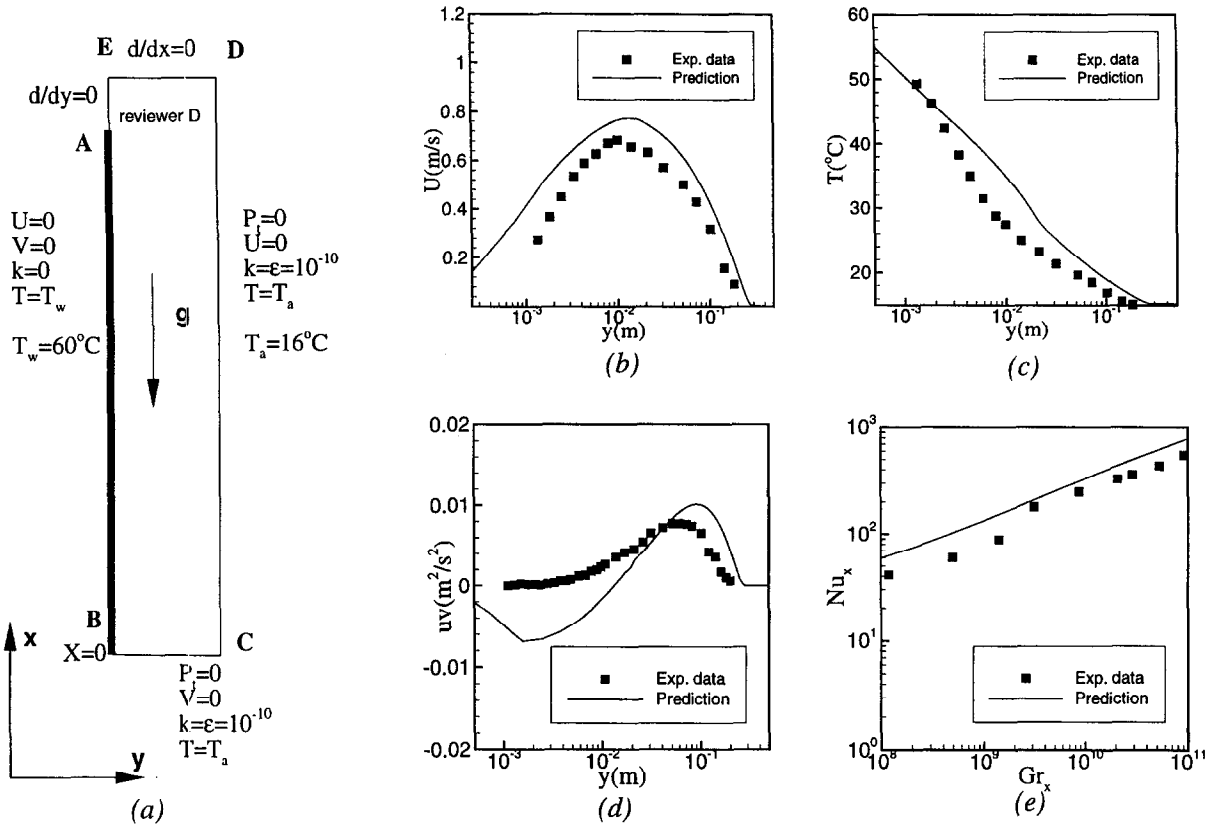

Fig. 5. Natural convection along a heated vertical plate (the data are from Tsuji and Nagano [9, 10]). (a) Geometry and boundary conditions; (c) mean temperature; (d) shear-stress; (e) local *Nu* number.

[1], gives surprisingly good agreement (1.2% error) with the DNS data. In this case, the two-layer model with y^*-prescription method reduces to the one-equation model since $y^* \leqslant 160$ everywhere.

The mean velocity and temperature in this case are asymmetrical and k and ε are symmetrical about the center line (dashed line in Fig. 1a). Results from the calculation using 10, 14, 20 and 40 grid points in the y direction are shown in Fig. 4. Figure 4a and b shows the mean velocity and temperature profile. The velocity has been non-dimensionalized by the characteristic velocity, $V_c = \sqrt{g\beta\Delta TL}$, and the temperature by the temperature difference ΔT. L represents the distance between two plates. These figures indicate that the new model predicts the meanflow well. The influence of grid number is negligible in the temperature and minimal in the velocity profile. Note that the position of the peak velocity is also well predicted. Fig. 4c and d illustrates the results for the non-dimensionalized k and ε. The absence of the gravity production term, as mentioned in previous section, leads to an under-prediction of k and ε by 20%. However, the trend of ε distribution in the immediate near-wall regions ($y/L < 0.05$ and $y/L > 0.95$) is correctly obtained, which confirm the model of l_ε given in equation (22). Fig 4e and f further compares the shear-stress computed by

$$\overline{uv} = -v_t \frac{\partial U}{\partial y} \tag{26}$$

and the turbulent heat flux by

$$\overline{vt} = -\frac{v_t}{pr_t}\frac{\partial T}{\partial y} \tag{27}$$

with the DNS results. Equation (26) predicts negative values for $\overline{uv}$ in $y/L < 0.05$ and $y/L > 0.95$, since both v_t and velocity gradient are positive in this region. The $\overline{uv}$ from DNS data, however, is positive in these regions. This discrepancy might be attributed to the counter-diffusion phenomenon. Figure 4f indicates that 10 grids gave poor results in turbulent heat flux. At least 14 grids are needed for this case.

The results suggest that, in the region where the one-equation model is applicable, i.e. $y^* < 160$, five grid points are sufficient to predict the mean flow. Better agreement for the turbulent quantities requires *seven–ten* grid points. Further increase of the grid number would not yield significant improvement in accuracy.

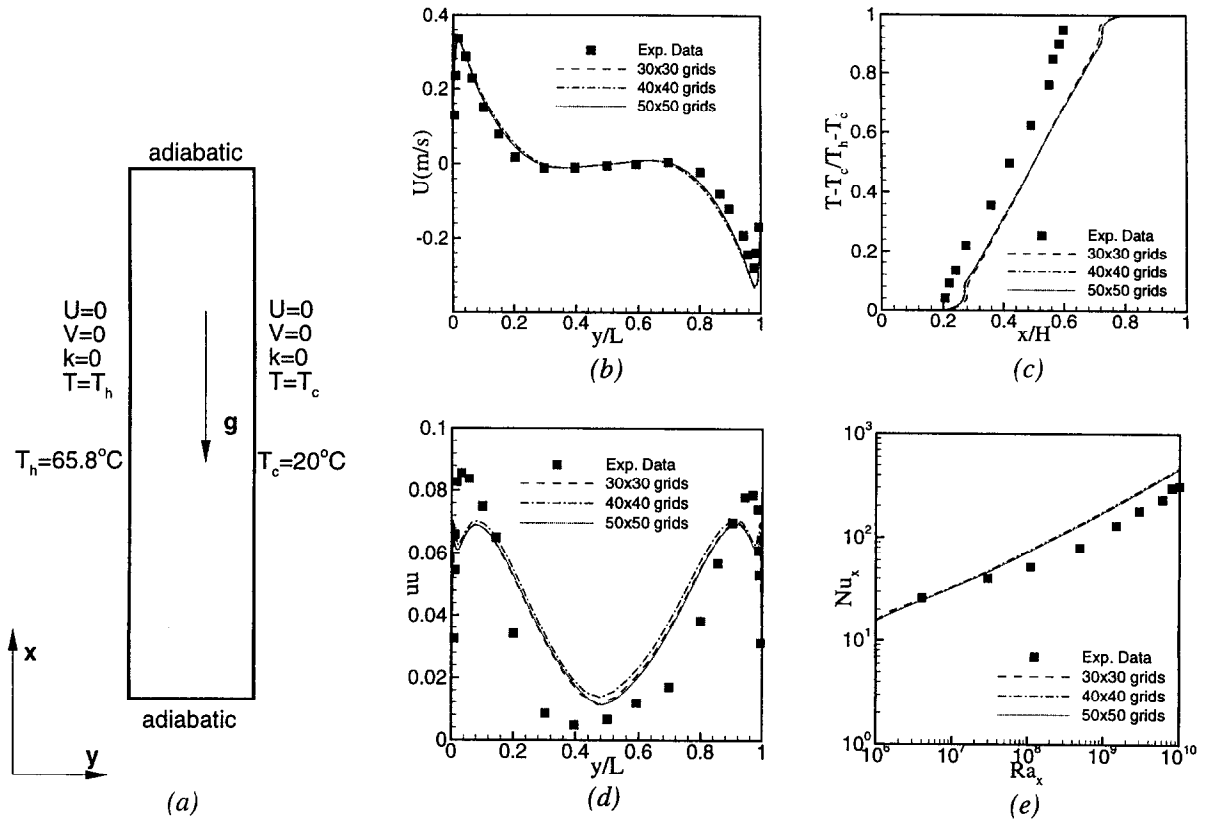

Fig. 6. Natural convection in a cavity with an aspect ratio 5 : 1 (the data are from Cheesewright et al. [16]). (a) Geometry and boundary conditions; (b) mean velocity at mid-height; (c) mean temperature in the core; (d) velocity fluctuation; (e) local *Nu* number.

3.2. *Natural convection along a heated, vertical, flat plate*

Figure 5a shows the plate sketch and a brief summary of the boundary conditions. The boundaries of the computation domain are identified by A, B, C, D and E. AB, BC, CD etc. are used hereafter to represent the physical boundaries between the points A and B, B and C, C and D, etc. respectively. Tsuji and Nagano [9, 10] performed detailed experimental studies for this case. They measured mean flow and some turbulence quantities at locations $x = 1.44$, 2.54, 3.24 m, etc., where x measured from the bottom of the plate.

Our computation used the boundary conditions suggested by Yuan [39], which were different from those used by To and Humphrey [1] and Henkes et al. [19]. To and Humphrey specified the laminar U and T profiles at $x = 0.05$ m and artificially introduced the turbulence quantities at a prescribed location: $Gr_x = 2 \times 10^9$. Henkes et al. used a similar method and even assumed $\nu_t/\nu = 20$ at the free boundary CD (see Fig. 5a). Hence, their studies presumed knowledge of this flow. In contrast, this study used stagnant conditions at the boundary BC and CD except that the normal velocities (U at BC and V at CD) were not specified. The total pressure P_t was fixed at zero at BC and CD. These specifications computationally allowed the flow to enter the domain through BC and CD as the buoyancy force drove the fluid out through DE. A very small value of k and ε (10^{-10}) was prescribed on BC and CD to initialize the turbulence calculation. CD is far from the plate so that the undisturbed conditions were applied. The fully developed conditions, $\partial/\partial x = 0$, were assigned to the boundary ED for all variables. EA is an extension of the plate designed for relaxing the end effect of the plate and used the symmetrical conditions. Finally, the wall AB adopted no-slip, zero k and fixed-temperature conditions.

These boundary conditions were adopted in the current study because they do not require any additional information, such as the transition location x_{cr} used in Refs [1, 19]. Since Tsuji and Nagano [9, 10] measured the velocities and temperature very close to the plate, the computation required a very fine grid (38×56) to compare the results with the experimental data. Still, this grid is much coarser than that used in Ref. [19], (72×80).

The results of the computation are shown in Fig. 5. Figure 5b–e compares the predicted results at $x = 2.54$

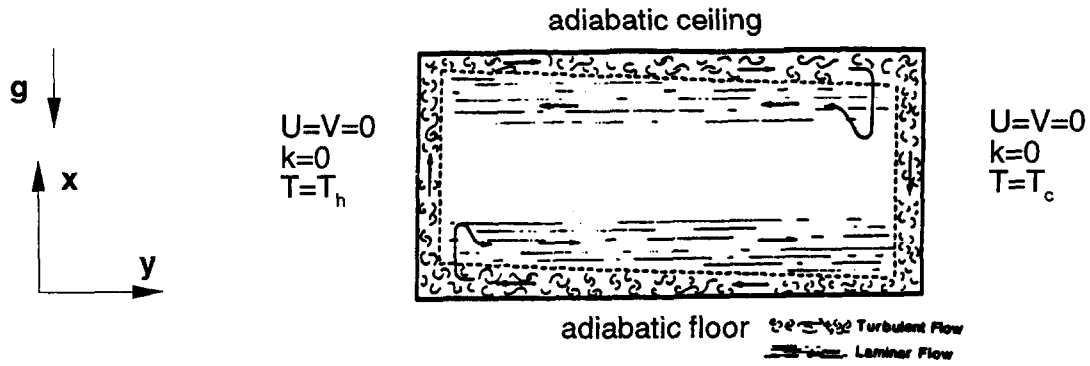

(a)

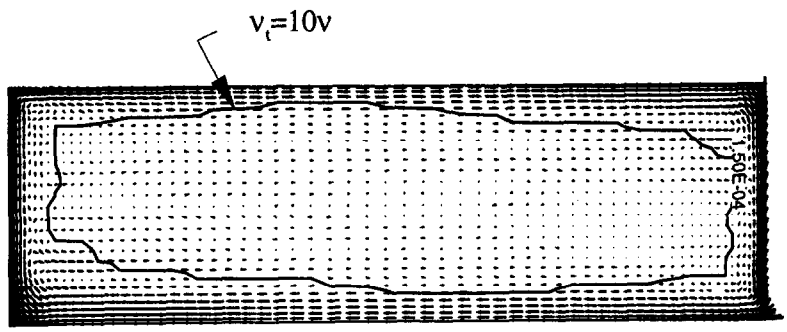

(b)

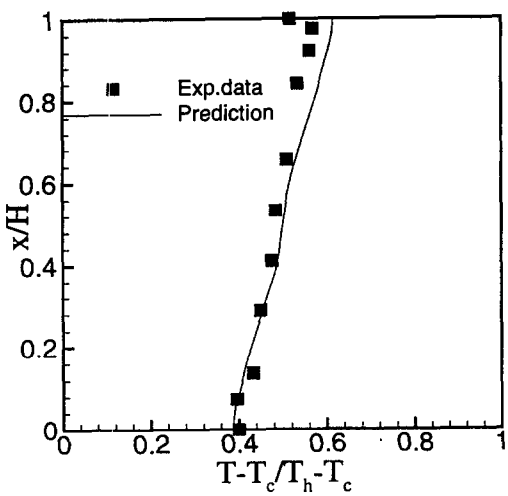

(c)

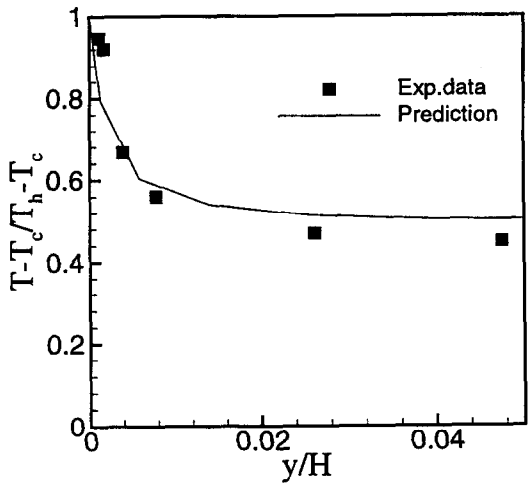

(d)

Fig. 7. Natural convection in a cavity with an aspect ratio of 2.5:7.9 (the data are from Olson et al. [17]). (a) Geometry, boundary conditions and flow pattern observed; (b) predicted flow pattern and turbulent region; (c) core temperature; (d) temperature at mid-height of the boundary layer.

Table 2
Computational details of four natural convection cases

Case	Computational object	Grid distribution $d_i/L=(i/N)^m$	Relaxation factors					
			U	V	P	T	k	ε
1	Two infinitely long parallel plates	10–40 grid points in y direction $m=1.5$	100	—	0.8	1	0.1	1
2	A 4 m × 1 m plate	30 grid points in x direction, $m=1$ 56 grid points in y direction, $m=1.5$	0.1	0.1	0.8	0.1	0.1	0.1
3	A 2.5 m × 0.5 m cavity	30–50 grid points in x direction, $m=1.8$* 30–50 grid points in y direction, $m=1.5$*	0.1	0.1	0.8	0.1	0.1	0.1
4	A 7.9 m × 2.5 m room	70 grids in x direction, $m=1.8$* 30 grids in y direction, $m=1.5$*	0.1	0.1	0.8	0.1	0.1	0.1

Notes: d_i: ith coordinate of the grid; L: full length of geometry in the specified direction i: grid index; N: total grid number in the specified direction; m: the spacing power. *The direction uses a symmetrical grid, consisting of power-law grid points that start at each end and meet in the middle.

m with the measured data from Tsuji and Nagano [9]. Figure 5b and c shows the mean-flow quantities. The two-layer model over-predicts the peak value of the velocity by about 10%. The temperatures predicted are within reasonable agreement with the experimental data but the discrepancy can be as large as 8°C in some areas. Figure 5d shows the shear stress calculated by equation (26). In the region where the velocity U is increasing with respect to y, i.e. $\partial U/\partial y > 0$, equation (26) calculated negative values of $\overline{uv}$, but the measurements give positive $\overline{uv}$. This effect might also be attributed to the counter-diffusion phenomenon. Figure 5e compared the computed and measured local Nusselt number. The computed values are higher than the experimental data. This discrepancy occurs because the two-layer model was used to calculate the entire plate even though only part of it was laminar. Particularly in the laminar region close to the leading edge, the use of a turbulence model in this region might predict an early transition which will enhance the heat transfer significantly. In fact, thew transition point was found 0.8 m above the leading edge in the experiments while the computation found the transition location to be only about 0.2 m above the edge.

3.3. Natural convection in a cavity with an aspect ratio of 5

Natural convection flows in cavities occur in many practical situations, such as rooms. In this section, natural convection in a tall cavity of 0.5 m width and 2.5 m height is investigated numerically with the new two-layer model. Cheesewright et al. [16] conducted experimental studies on natural convection in this cavity. Their experiments maintained isothermal conditions (65.8°C and 20°C) on the two vertical walls and insulated the two horizontal walls, although, they were not ideally insulated. The Rayleigh number based on cavity height was 5×10^{10}.

Figure 6a shows the geometry and boundary conditions adopted in the numerical simulation for this case. The numerical simulation uses the isothermal boundary condition for the two vertical walls and adiabatic conditions for the horizontal walls. No-slip and zero-k conditions were applied at all walls. Again no boundary condition for ε was necessary since ε is determined by equation (20) in the boundary layer.

Figure 6b compares the computed and measured mean velocity at the mid-height of the cavity. The computed velocity profile agrees with the experimental data. The measured velocities are not absolutely symmetrical about the center point because of the imperfect insulation on the horizontal walls. The predicted core temperatures, as shown in Fig. 6c, are higher than the measurements. This also may be attributed to the imperfect insulation on the horizontal walls that may lead to a heat loss from the cavity to the lab environment. Hence, the measured core temperatures were relatively lower. Even so, the computed and measured temperature gradients in the core region are similar. Figure 6d shows the velocity fluctuations at the mid-height. Only qualitative agreement is found between the computed results and the measured data. Lankhorst and Hoogendoorn [23] pointed out the deviations of this sort are due to the non-isotropic effects near the velocity maximum. The eddy-viscosity models assumed isotropic turbulence (equation (8)), which is certainly not the case near the velocity maximum. If the vertical component of the velocity fluctuation is larger than two horizontal components, better agreement between the numerical simulations and measurements can be expected with the increase of the factor 2/3 in equation (8). The computed local Nusselt number profile, as shown in Fig. 6f, agrees with the measured data.

In addition, a grid-dependency study for this case has been conducted with three sets of grids: 30×30, 40×40 and 50×50. Figure 6b–e indicates that the results with 50×50 grid points and 30×30 grid points has negligible

differences. This suggests that 30×30 grids are sufficient. Lankhorst et al. [23] mentioned that, for Rayleigh numbers of the order 10^{10}, a minimal mesh of 45×45 grid points is needed with the standard KEM. Chen [40] compared the performance of five difference turbulence models for this case and used 60×40 grids with the standard KEM and 100×60 with a LRN KEM. It is obvious that the new two-layer model can save computational costs significantly.

3.4. Natural convection in a room with an aspect ratio of 2.5 : 7.9

This section will explore the natural convection in a room 2.5 m in height, 7.9 m in width and 3.9 m in depth where Olson et al. [17] conducted experiments. In their experiments, two vertical walls were maintained isothermally at 20.3°C and 10.9°C, and the horizontal walls were well insulated. Since the front and back walls were also well insulated, the symmetry plane can be treated as a 2-D case. The Rayleigh number based on the room height was about 3×10^{10}. Olson et al. observed the flow pattern and measured the temperature distribution in the core region and in the vertical boundary layers. They recorded reverse flows along the ceiling and floor, which is rarely found in tall cavities.

The boundary conditions used in the present 2-D numerical simulations are: fixed temperature at the two vertical walls and adiabatic on the horizontal walls. No-slip and zero-k conditions again apply to all walls. Xu and Chen [41] found that radiation between ceiling and floor could result in some local changes of the flow pattern in the lower-left corner and upper-right corner. The current study employed a surface-to-surface radiation model to consider the radiation effects. The computation used 30×70 grids in the x and y directions respectively.

Figure 7a and b shows the observed and predicted flow pattern. The reverse flows were successfully predicted by the numerical simulation. The present computation found weak turbulence in the near-wall region. The contour $\nu_t = 10\nu$ shown in Fig. 7b, is close to the turbulent region sketched in Fig. 7a. The temperature profiles in the core region and in the vertical boundary layers are compared with the experimental data in Fig. 7c and d with good agreement. Hanjalic et al. [24] obtained a similar flow pattern by using a three-equation and a four-equation model but they could not find any turbulence. Xu and Chen [41] systematically computed this case by using LRN KEMs, and obtained a similar flow pattern and temperature distributions but used a much larger grid number (60×96). Again the two-layer model is found to be both cost-effective (only 30×70 grids) and reasonably accurate.

4. Conclusions

Based on the analysis of a direct numerical simulation of natural convection, this study has developed a new near-wall, one-equation turbulence model for calculating the natural convection boundary layer. A new two-layer model is then formed by applying the new one-equation model in the region where $y^* \leqslant 160$ and the standard k–ε model where $y^* > 160$. The two-layer model requires only 7–10 grids to simulate natural convection boundary layer. The computing cost is much less than that of a low-Reynolds number k–ε model or a Reynolds-stress model.

The two-layer model has been applied to calculate four natural convection flows: flows in a vertical slot, along a vertical, heated, and flat plate and in two cavities. The applications confirmed that the model can predict natural convection accurately and efficiently.

References

[1] To WM, Humphrey JAC. Numerical simulation of turbulent buoyancy, turbulent flow—I. Free convection along a heated, vertical, flat plate. Int. J. Heat Mass Transfer 1986;29:573–92.

[2] Versteegh TAM, Nieuwstadt FTM. Scaling of free convection between two differentially heated infinite vertical plates. In: Turbulent Shear Flow 1996;11.

[3] Launder BE, Spalding DB. The numerical computation of turbulent flows. Computer Methods in Applied Mechanics and Energy 1996;3:269–89.

[4] Warner CY, Arpaci VS. An experimental investigation of turbulent natural convection in air at low pressure along a vertical heated flat plate. Int. J. Heat Mass Transfer 1968;11:397–406.

[5] Cheesewright R. Turbulent natural convection from a vertical plane surface. J. Heat Transfer 1968;90:1–8.

[6] Smith RR. Characteristics of turbulence in free convection flow past a vertical plate. Ph.D. Thesis, University of London 1972.

[7] Cheesewright R, Doan KS. Space time correlation measurements in a turbulent natural convection boundary layer. Int. J. Heat Mass Transfer 1978;21:911–21.

[8] Miyamoto M, Okayama M. An experimental study of turbulent free convection boundary layer in air along a vertical plate using LDV. Bull. J.S.M.E. 1982;25:1729–36.

[9] Tsuji, Nagano. Turbulence measurements in a natural convection boundary layer along a vertical flat plate. Int. J. Heat Mass Transfer 1988;31:2101–11.

[10] Tsuji, Nagano Y. Characteristics of a turbulent natural convection boundary layer along a vertical flat plate. Int. J. Heat Mass Transfer 1989;31:1723–34.

[11] Yuan X, Moser A, Suter P. Wall functions for numerical simulation of turbulent natural convection along vertical plates. Int. J. Heat Mass Transfer 1993;36:4477–85.

[12] Laurence D, Dauthieu I, Bouchama N. Proc. 5th ERCOFTAC/IAHR Workshop on Refined Flow Modeling. April 25–26 1996;Chatou-Paris.

[13] Elder JW. Turbulent free convection in a vertical slot. J. Fluid Mech. 1965;23:99–111.

[14] Giel PW, Schmidt FW. An experimental study of high Rayleigh number natural convection in an enclosure. Pro-

ceedings of the 8th International Heat Transfer Conference, vol. 4, 1986; pp. 1459–64.

[15] Cowan GH, Lovegrove PC, Quarini GL. Turbulent natural convection. Proceedings of the 7th International Heat Transfer Conference 1982; pp.195–203.

[16] Cheesewright R, King KJ, Ziai S. Experimental data for validation of computer codes for the prediction of two-dimensional buoyant cavity flows. In: Significant Questions in Buoyancy Affected Enclosure or Cavity Flows by J. A. C. Humphrey et al., editors. 75–81, ASME Winter Annual Meeting, 1986.

[17] Olson, DA, Glicksman LR, Ferm HM. Steady-state natural convection in empty and partitioned enclosures at high Rayleigh numbers. J. Heat Transfer, Trans. ASME 1993;112:640–7.

[18] Dafa'Alla AA, Betts PL. Turbulent natural convection in a tall cavity. Experimental Heat Transfer 1996;9:165–94.

[19] Henkes RAWM, Hoogendoorn CJ. Comparison of turbulence models for the natural convection boundary layer along a heated vertical plate. Int. J. Heat Mass Transfer 1989;32:157–69.

[20] Peeters TWJ, Henkes RAWM. The Reynolds-stress model of turbulence applied to the natural-convection boundary layer along a heated vertical plate. Int. J. Heat Mass Transfer 1992;35:403–20.

[21] Henkes RAWM, Van Der Vlugt FF, Hoogendoorn CJ. Natural-convection flow in a square cavity calculated with low-Reynolds-number turbulence models. Int. J. Heat Mass Transfer 1991;34:377–88.

[22] Chen Q. Prediction of Room Air Motion by Reynolds-Stress Models. Building and Environment 1996;31:233–44.

[23] Lankhorst AM, Hoogendoorn CJ. Numerical computation of high Rayleigh number natural convection and prediction of hot radiator induced room air motion. Applied Scientific Research 1989;47(4):301–22.

[24] Hanjalic K, Kenjereš, S, Durst, F. Natural convection in partitioned two-dimensional enclosures at higher Rayleigh numbers. Int. J. Heat Mass Transfer 1996;39:1407–27.

[25] Phillips JR. Direct simulations of turbulent unstratified natural convection in a vertical slot for $Pr = 0.71$. Int. J. Heat Mass Transfer 1996;39:2485–94.

[26] Paolucci S. Direct numerical simulation of two dimensional turbulent natural convection in an enclosed cavity. J. Fluid Mech. 1990;215:229–62.

[27] Xin S, Le Quéué P. Numerical simulation of 2D turbulent natural convection in differentially heated cavities of aspect ratios 1 and 4. In: Direct and Large-Eddy Simulation I. P. R. Voke et al. editors. Kluwer Academic Publishers, 1994, pp. 423–34.

[28] Boudejemadi R, Maupu V, Laurence D, Le Quéué P. Budgets of turbulent stresses and fluxes in a vertical slot natural convection flow Rayleigh $Ra = 10^5$ and $5.4\,10^5$. Int. J. Heat Fluid Flow 1997;18:70–9.

[29] Dol HS, Hanjalic K, Kenjereš S. A comparative assessment of the second-moment differential and algebraic models in turbulent natural convection. Int. J. Heat Fluid Flow 1997;18:4–14.

[30] Hammond GP. Turbulent Prandtl number within a near-wall flow. AIAA J. 1985;23:1668–9.

[31] Mason HB, Seban RA. Numerical predictions for turbulent free convection from a vertical plate. J. Heat Transfer 1974;17:1329–36.

[32] Plumb OA, Kennedy LA. Application of a k-ε turbulence model to natural convection from a vertical isothermal plate. J. Heat Transfer 1977;99:79–85.

[33] Hanjalic K, Vasic S. Computation of turbulent natural convection in rectangular enclosures with an algebraic flux model. Int. J. Heat Mass Transfer 1993;26:3603–24.

[34] Norris LH, Reynolds WC. Turbulent channel flow with a moving wavy boundary. Rept. No. FM-10. Stanford University, Dept. of Mech. Eng. 1975.

[35] Rodi W. Experience with two-layer models combing k-ε model with a one-equation model near the wall. Paper AIAA 91-0216 (1991).

[36] Durbin PA. Near-wall turbulence closure without damping functions. Theoretical and Computational Fluid Dynamics 1991;3:1–13.

[37] Rodi W, Mansour NN, Michelassi V. One-equation near-wall turbulence modeling with the aid of direct simulation data. J. Fluid Engineering, Transactions of the ASME 1993;115:196–205.

[38] Spalding DB. The PHOENICS Encyclopedia. CHAM, Ltd., London, U.K. 1994.

[39] Yuan X. Wall functions for numerical simulation of natural convection along vertical surfaces, Ph.D Thesis, Swiss Federal Institute of Technology, Zurich, Switzerland, 1995.

[40] Chen Q. Comparison of different k-ε models for indoor air flow computations. Numerical Heat Transfer, Part B 1995;28:353–69.

[41] Xu W, Chen Q. Numerical simulation of natural convection in a room with differentially heated vertical walls. ASHRAE Trans 1998;104(1).